2006:273 CIV

MASTER'S THESIS

Temperature Stabilization of Electronics Module

Anders Gabert

Luleå University of Technology

MSc Programmes in Engineering
Electrical Engineering
Department of Computer Science and Electrical Engineering
Division of EISLAB

2006:273 CIV - ISSN: 1402-1617 - ISRN: LTU-EX--06/273--SE

Temperature stabilization of electronics module

Anders Gabert

Luleå University of Technology
Dept. of Computer Science and Electrical Engineering
EISLAB

25th of September 2006

ABSTRACT

Outdoor applications of electronics modules expose the systems to harsh environmental conditions. When very high performance is required, it may be necessary to actively stabilize the temperature in the module. This thesis presents a systematic approach to the problem of designing a temperature stabilized environment for medium size electronics modules.

The target system is the front-end electronics for the antennas in the EISCAT_3D incoherent scatter radar system. This will be placed in northern Scandinavia, with estimated outdoor temperature span from -40°C to 40°C. Very high demands on precision and timing will most likely require a temperature stable environment. The present state in high performance thermal management of electronics focuses on single circuit design. Thus the need of designing a temperature stable module which could hold the entire front-end electronics was recognized. The electronics have an estimated constant power dissipation of about 10 W.

The temperature stabilization system consists of a 250x250x100 mm large aluminium box insulated on the outside. Two Peltier modules are used for active cooling and heating. Inside the box a 10 mm thick aluminium heat spreader is attached to the Peltier modules. The heat spreader is used both as a mount for the most temperature critical components, as well as a means to distribute heating and cooling inside the box. Also the aluminium casing itself is used to distribute heat energy evenly. The current through the Peltier modules is controlled using a PID controller acting on a linearly controlled H-bridge.

The system was initially evaluated using FEM simulations. The simulations verified the design approach and gave a clear picture of the heat distribution in the box over the range of target temperatures. Measurements were made on the prototype system using a climate chamber in which the prototype box was exposed to temperatures from 40°C down to -40°C over a time period of 5.5 hours. Inside the box two power resistors were used to generate the estimated power dissipation of 10 W. The measurements show that the center of the heat spreader is kept at 20°C with minor deviations of ±0.02°C. The air inside the box measured 45 mm above the aluminium heat spreader shows temperature variations of ±5°C.

Both simulations and measurements clearly show the feasibility of the proposed design, with temperatures kept to close tolerances. Critical parts can be attached to the aluminium heat spreader while less critical can be positioned above. The use of a completely enclosed box without rotating parts should provide long life expectations.

Preface

The work presented in this master's thesis was carried out at the Embedded Internet System Laboratory (EISLAB) at Luleå University of Technology. The work was part of the four year design study EISCAT_3D which aims to develop a new incoherent scatter radar system for the EISCAT Scientific Association. EISLAB is here responsible for the front-end electronics of the new system.

I would like to thank everyone that has supported me during this thesis. Special gratitude's to, my supervisor Jonny Johansson for his great support and for taking time to help me, and to Johan Borg for many helpful ideas and valuable comments during this work.

The work presented in this master's thesis was funded by the European Community under the "Structuring the European Research Area" Specific Programme Research Infrastructures action.

Anders Gabert

Contents

Chapter 1: Introduction 1
1.1 Background of the EISCAT_3D project 1
1.2 Purpose 2
1.3 Introduction to this thesis 3

Chapter 2: Theory 5
2.1 Basic thermodynamics 5
2.2 Thermoelectric Modules 6
2.3 Sensors 10

Chapter 3: Simulations 13
3.1 Model of the Peltier module 13
3.2 Model of the box and Peltier modules 14

Chapter 4: Thermal Management Box 19
4.1 The module 19
4.2 Temperature controller 20
4.3 Matlab GUI 24

Chapter 5: Final Evaluation of the Finished Prototype 25
5.1 Evaluation with ambient temperature changes 26
5.2 Evaluation of recovery from power dissipation changes 28
5.3 Evaluation of stability at constant power dissipation 28

Chapter 6: Discussion and Future Work 33
6.1 Discussion 33
6.2 Future work 34

CHAPTER 1

Introduction

1.1 Background of the EISCAT_3D project

The EISCAT Scientific Association is an international research organisation operating three incoherent scatter radar systems, at 224 MHz, 500 MHz and 931 MHz, in northern Scandinavia. The EISCAT (European Incoherent Scatter) radar system is used for studies of the interaction between the Sun and the Earth as revealed by disturbances in the magnetosphere and the ionised parts of the atmosphere (these interactions also give rise to the spectacular aurora, or Northern Lights). The EISCAT radar system consists of a transmit and receive site located close to the city of Tromsø, in Norway, and additional receiver stations are located in Sodankylä, Finland, and Kiruna, Sweden. There is also a second incoherent scatter radar facility, the EISCAT Svalbard Radar, located on the island of Spitsbergen, far to the north of the Norwegian mainland [1].

The radars of the EISCAT Scientific Association have defined the state of the art within the World's incoherent scatter community for the last several years. To maintain Europe's future world leadership role in this field, a new incoherent scatter radar system needs to be developed. Therefore the EISCAT Scientific Association, in co-operation with the University of Tromsø, Norway, Luleå University of Technology, Sweden, and the Rutherford Appleton Laboratory, United Kingdom, has started a four year design study named EISCAT_3D funded by the European Community. The new incoherent scatter radar system will be based on large phased array systems. The new system consists of an antenna array for both transmission and reception, together with two further remote reception facilities [2].

The main responsibility of EISLAB at Luleå University of Technology lies in the front-end electronics for each antenna element in the array. This involves synchronization between array elements, low noise RF front-end design and high speed A/D converter design. High demands are put on precision and timing. In table 1.1 some of these demands are listed.

Table 1.1: Specifications of the antenna front-end electronics.

Dynamic range	80 dB
Time tolerance between antenna element	± 50 ps
Total receiver noise figure	0.7 dB
Receiver gain	60 dB
Signal frequency	225 MHz
Signal bandwidth	30 MHz
Phase linearity	1°

The front-end electronics will be positioned as close to the antennas as possible. This will expose the system to the harsh outdoor environmental conditions of northern Scandinavia, with an estimated outdoor temperature span from -40°C to 40°C. The harsh environment together with the high demands on precision and timing on the electronics involved will most likely require a temperature stable environment for the front-end electronics. Thus, this master's thesis has been initiated to investigate the possibility to temperature stabilize one antenna front-end including filter, amplifiers, A/D converters and time synchronization.

1.2 Purpose

The purpose of this master's thesis is to design and build a temperature stabilization system for the front-end electronic module of the new EISCAT_3D phased array system. The system should stabilize the temperature of the front-end electronics at a desired temperature of 20°C, with ambient temperature ranging from -40°C to 40°C. The electronics have an estimated constant power dissipation of about 10 W. The aim is to investigate which temperature stability can be achieved if Peltier modules are used as the active device.

In the beginning of the thesis some guidelines were given regarding the design of the system, these guidelines are listed below.

- The system will use active cooling and heating (e.g. Peltier modules) controlled by an autonomous electronic system.

- No mechanically moving parts are allowed, this to guarantee long life stability. Thus only natural convection (no fans) is used.

- A closed system architecture, the box should be completely enclosed.

1.3 Introduction to this thesis

As previously stated the purpose of the thesis project is to build a temperature stabilization system for the front-end electronics of the new EISCAT_3D radar system. The present state in high performance thermal management of electronics modules focuses on using some sort of mechanical system, like forced convection by direct air cooling using fans or liquid-cooling. This because of the high efficiency of these systems [3]. When high temperature stability is needed the attention is directed at single circuits.

In March 2003 Arthur E. Bergles published a paper on the evolution of cooling technology for electrical equipment, ranging from the early days of electronic tubes to present trends in thermal management. He states that in the 1970s the thermal technology rapidly advanced with the development of integrated circuits. With very large scale integration the number of components per chip increased to over 100 000 by the end of the decade. The decreases in power dissipation at each gate became overwhelmed by the increase in the number of gates. Because the increase in chip size was modest the heat fluxes steadily increased. This gave birth to new and advanced methods of thermal management [3]. In 1968 Larsen published a paper on the construction of a temperature controller achieving a stability of a water bath within 50 μ°C. Using a platinum resistor in an AC-excited bridge made the sensitivity of the controller approach the theoretical limitation imposed by Johnson noise [4]. In 1996 A W Sloman described the temperature stabilization of the surface of the resonant mirror sensor used in the IASys biosensor unit, used for measuring the refractive index of a surface. The system keeps the temperature stable within ±1 m°C in the range of 4-38°C using a Peltier module attached to the mirror sensor. The control system is a PID controller implemented on a microcontroller and the Peltier module is driven using a PWM signal [5]. Luciano Di Fiora describes a temperature control for a laser diode using a NTC thermistor and a Peltier thermoelectric module obtaining a temperature stability of ±20 μ°C over a period of 1h 44min. The Peltier module was driven using a linear output stage [6].

The EISCAT_3D front-end consists of several active and passive components that should be housed in an enclosed module. Thus, the need for a temperature stabilized module which could hold the entire front-end electronics was recognized. The module should provide a completely enclosed environment for the electronics without moving parts, this to guarantee long life expectations. From this the aim of constructing a temperature stabilized box grows which could contain the entire front-end electronics. If the module is properly insulated it should be possible to achieve a good temperature stable environment for the electronics.

In the following chapter's theory, simulations and detail about the construction of the module will be discussed. The thesis will then end in an evaluation and discussion about the final prototype.

Chapter 2
Theory

2.1 Basic thermodynamics

To get an understanding of the processes involved in thermodynamics, some basic definitions will be discussed. The heat transfer from a load to the ambient environment is a function of two thermal processes, conduction and convection.

Conduction is the thermal flow of heat through matter. It is a function of the temperature difference across the material, the physical dimensions and the thermal conductivity of the material. The numerical value of the thermal conductivity indicates how fast heat will flow in a given material. Materials used for transferring heat should have a high thermal conductivity and insulation materials should have a low thermal conductivity. Table 2.1 lists typical values of the thermal conductivities for some materials, in general the thermal conductivity is strongly temperature-dependent [7]. The thermal heat transfer through a material can be described by the following function

$$Q_d = -\frac{kA}{\Delta x}(T_2 - T_1). \tag{2.1}$$

Where Q_d is the amount of heat conducted in W, Δx is the thickness of the material in m, A is the exposed surface area of the material in m^2, $(T_2 - T_1)$ is the temperature difference between opposite sides of the material in °C and k is the thermal conductivity of the material in W/m°C [7].

Table 2.1: Approximate values of thermal conductivity.

	Temperature °C	Thermal conductivity k, W/mK
Air	20	0.025
Aluminium	20	204
Copper	20	386
Iron	20	73
Steel	20	54
Glass Wool, 24 kg/m^3	23	0.038
Silica aerogel	32	0.024
Polystyrene (Styrofoam)	25	0.027

Convection is the heat transfer across the boundary layer of air at the surface of a material. It's a function of the temperature difference across the boundary layer and the rate of air movement at the surface. The faster the air moves the greater the convection of heat is. Table 2.2 shows approximate values of convection Heat-transfer coefficients in air [7]. Newton's law of cooling expresses the effects of convection

$$Q_v = hA(T_w - T_{amb}). \tag{2.2}$$

Where Q_v is the amount of heat transferred by convection in W, A is the exposed surface area of the material in m^2, $(T_w - T_{amb})$ is the temperature difference between the material and the ambient air and h is the convection heat-transfer coefficient [7].

Table 2.2: Approximate values of convection heat-transfer coefficients.

Mode	h, W/m^2K
Free Convection, $\Delta T = 30$°C	
Vertical plate 0.3 m high in air	4.5
Horizontal cylinder, 5 cm diameter, in air	6.5
Forced convection	
Airflow at 2 m/s over 0.2 m square plate	12
Airflow at 35 m/s over 0.75 m square plate	75

2.2 Thermoelectric Modules

The thermoelectric or Peltier module is an electrical module that functions as a heat pump when an electrical current is passed through the module. When a DC current is applied to the module, heat is moved from one side of the module to the other, creating

a cold and a hot side. The operation of the thermoelectric devices can be associated with four physical phenomena: the Seebeck effect, the Peltier effect, the Thomson effect, and the Joule effect.

2.2.1 Seebeck Effect

Thomas J. Seebeck discovered in 1821 that when two conductors of different material are connected and if the junctions are maintained at different temperatures, an emf (Electromotive force) can be measured in the circuit. The emf generated is known as the Seebeck effect. The open-circuit voltage is a function of the materials and the temperature of the two junctions [8].

$$V_{ab} = C_1(Th - Tc) + \frac{C_2}{2}(Th - Tc)^2 \tag{2.3}$$

The Seebeck coefficient is defined as

$$a_{ab} = \frac{\partial V_{ab}}{\partial Th} = C_1 + C_2(Th - Tc) + C_3(Th - Tc)^2. \tag{2.4}$$

2.2.2 Peltier Effect

In 1834 Jean C.A. Peltier discovered that when an electrical current passes through a junction of two different conductors in a certain direction a cooling effect is produced, and in opposite direction, a heating effect. Both the heat generated and absorption is proportional to the current and dependent on the temperature of the junction [8]. The Peltier effect is expressed as

$$Q_p = \Pi_p I. \tag{2.5}$$

Here Π_p is the Peltier coefficient of the junction representing how much heat is carried through a given material. Thomson's second relation describes a relation between the Peltier and Seebeck coefficients [9]

$$\Pi_p = -aT \tag{2.6}$$

where a is the Seebeck coefficient of the two different conductors and T is the absolute temperature at the junction, equation (2.5) can then be written as

$$Q_p = -aTI. \tag{2.7}$$

2.2.3 Thomson Effect

William Thomson (Lord Kelvin) examined both the Seebeck and Peltier effects and derived a relation between the coefficients.

In the process, he predicted the existence of a new effect called the Thomson effect. In the Thomson effect, heat is absorbed or produced when current flows in a material with

a temperature gradient. The heat is proportional to both the electric current and the temperature gradient. The Thomson effect per unit volume is written as

$$q_t = \tau J \frac{dT}{dx}, \tag{2.8}$$

where τ is the Thomson coefficient, J is the current density and $\frac{dT}{dx}$ is the temperature gradient [10].

2.2.4 Joule Effect

Joule heat is generated when an electrical current is passed through an isothermal conductor. Joule heat per unit volume is written as

$$q_j = \rho J^2 \tag{2.9}$$

where ρ is the electrical resistivity and J is the current density. This process is irreversible and when operating condition of thermoelectric devices there is another irreversible process, thermal conduction [8].

2.2.5 Structure of Thermoelectric Modules

The typical thermoelectric module is composed of P-type and N-type Bismuth Telluride dice that are sandwiched between two ceramic substrates. The ideal material to use when constructing thermoelectric modules has a high Seebeck coefficient and low electrical resistivity, small amounts of heat is generated from the electrical current flow, and low thermal conductivity. Therefore a small amount of heat is transferred from the hot side to the cold side. The dice are connected in series and thermally in parallel. The number of dice in one module is dependent on its size and efficiency. A typical module with the dimension 30x30 mm consists of about 100 dice. The modules can also be made in stacked multi-stage modules to improve efficiency [11]. Figure 2.1 shows an illustration of a Peltier module.

The operation of the Peltier module is often described by three equations [10]. The heat pumped at the cold Q_c side is given by:

$$Q_c = a_m I T_c - \frac{1}{2} I^2 R_m - K_m (T_h - T_c) \tag{2.10}$$

where a_m is the Seebeck coefficient, R_m is the electrical resistance, K_m is the thermal conductance, I is the current through the Peltier, T_c is the temperature of the cold side, and T_h is the temperature of the hot side. The heat rejected from the hot side Q_h is given by:

$$Q_h = a_m I T_h + \frac{1}{2} I^2 R_m - K_m (T_h - T_c). \tag{2.11}$$

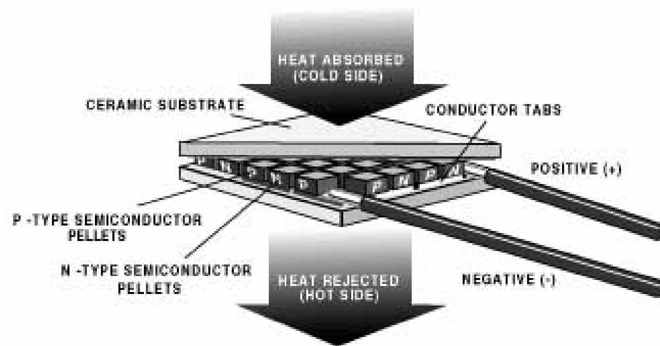

Figure 2.1: Illustration of a Peltier module, from [11].

The voltage across the Peltier module is given by:

$$V = a_m(T_h - T_c) + IR_m. \tag{2.12}$$

These equations show, the function of the Peltier module is dependent on the temperature difference over the module $(T_h - T_c)$. This is because of the thermal conductance of the Peltier material. Heat will transfer from the hot side of the Peltier to the cold side and as the temperature difference increases, the heat transferred will increase until a state of equilibrium is reached. For the Peltier to carry on working the current must be increased. However, for every increase in current there is another equilibrium. Each Peltier has a maximum operational current which gives the maximum temperature difference for the Peltier module. Single-stage modules can keep a temperature difference of about 75°C and the maximum operation temperature is +80°C. Special high temperature modules have a much higher operation temperature of up to +120°C and higher.

2.2.6 Power Control for Thermoelectric Modules

There are two approaches to power a thermoelectric module; pulse-width modulation (PWM) and linear control. The most efficient is the pulse-width modulation, because the driving transistors are either fully opened or closed. This means that very little power is dissipated within the transistor. The pulse-width modulation frequency is recommended to be 2 kHz or higher, this because low frequencies are more thermally stressful to the thermoelectric module than high frequencies. Despite the advantage with PWM, it cannot always be used because of the potential for electromagnetic interference (EMI). The high current pulses can cause high frequency noise. In these instances a linear drive circuit is engaged to vary the current level. Unfortunately this circuit will dissipate a lot more power than a pulse-width-modulated [11].

2.3 Sensors

2.3.1 Resistive Temperature Detectors

Resistive temperature detectors or RTD is a resistive temperature detector fabricated either in the form of a wire or a thin film. The most common material to make RTDs of is platinum because of its predictable response, long-term stability, and durability [12].

The conductive material which the RTDs are made of has a positive temperature coefficient, which means that the resistance increases when the temperature rises. In a conductor the number of electrons available to conduct electricity does not significantly change with temperature. But when the temperature increases, the vibrations of the atoms around their equilibrium positions increase in amplitude. This results in a greater dispersion of electrons, which reduces their average speed. Hence, the resistance increases when the temperature rises [13].

The advantages of RTDs are their high repeatability, high sensitivity, long-term stability and the accuracy of platinum. The relationship between the resistance and temperature can be described by Callendar-van Dusen approximations for platinum. In industry, it is customary to use separate approximations for the cold and hot temperatures. For the range from -200°C to 0°C,

$$R_t = R_0 \left[1 + At + Bt^2 + Ct^3(t - 100)\right]. \tag{2.13}$$

For the range from 0° C to 630° C,

$$R_t = R_0(1 + At + Bt^2). \tag{2.14}$$

The constants A, B, and C are determined by the properties of platinum used in the sensor, R_0 is the Nominal resistance at 0°C [12].

2.3.2 Thermistors

The name thermistors comes from "thermally sensitive resistor". They are based on semiconductors and not on conductors as the RTD. There are two different types of thermistors, the PTC with a positive temperature coefficient and the NTC with a negative temperature coefficient. Michael Faraday described the first thermistor in 1833.

Thermistors are based on the temperature dependence of a semiconductor's resistance, which is due to the variation in the number of available charge carriers and their mobility. When the temperature increases, the number of charge carriers also increases and the resistance decreases, thus yielding a negative temperature coefficient. This dependence varies with the impurities and when the doping is very heavy, the semiconductor achieves metallic properties and shows a positive temperature coefficient over a limited temperature range [13].

Only the NTC thermistors are useful for precision temperature measurements [12]. The resistance of a NTC thermistor is determined by its physical dimensions and the

resistivity of the material. The relationship between the resistance and temperature is highly nonlinear. Over a 50°C span the relationship is almost exponential and can be expressed as

$$R_T = R_0 e^{\beta(1/T - 1/T_0)} \tag{2.15}$$

where R_0 is the resistance at a reference temperature T_0 which is given in Kelvin. β is the characteristic temperature of the material and its value, which is temperature-dependent usually ranges from 2000 K to 4000 K [13]. The thermistor is less time stable than the RTDs, and time stability is obtained by artificial aging. Interchange-ability is only guaranteed for special models.

Thermistors have many advantages and are extensively used. Their high sensitivity gives a high resolution when measuring temperature. Their high resistivity permits small mass units with fast response and long connecting wires [13].

2.3.3 Self-Heating Effect in Temperature sensors

The resistive temperature sensor require an excitation signal for its operation, the signal is usually either dc or ac passing through the sensor. This electric current causes a Joule heating which will increase the sensor temperature. In many applications this is a source of error which may result in an erroneous determination of the temperature. The self-heating effect can be used for example when sensing fluid flow and thermal radiation.

The temperature error caused by self-heating can be calculated using equation (2.16) which gives the temperature increment above ambient temperature when dissipating a power P_S in the sensor. Here δ is the dissipation capability of the sensor in a given environment and is called the heat dissipation constant or heat dissipation factor [13].

$$\Delta T = \frac{P_S}{\delta} = \frac{I^2 R}{\delta} \tag{2.16}$$

CHAPTER 3

Simulations

To get an idea on the thermal behaviour of the module a simulation model was made in COMSOL Multiphysics^{TM}. The simulation model consists of the box and a model of the Peltier module used to drive the thermal system.

3.1 Model of the Peltier module

To simulate the function of a Peltier module a simple model is made. The model is based on the constant parameter theory equation. These equations assume that the thermoelectric parameters a_m the Seebeck coefficient R_m, the electrical resistance and K_m the thermal conductance are invariant with temperature. This assumption only holds for very small $(T_h - T_c)$, where T_h is the hot side temperature and T_c is the cold side temperature of the Peltier module. Rowe points out that the equations are useful but not accurate, but they will still give a useful approximation of the Peltier module [10].

$$Q_c = a_m I T_c - \frac{1}{2} I^2 R_m - K_m (T_h - T_c) \tag{3.1}$$

$$Q_h = a_m I T_h + \frac{1}{2} I^2 R_m - K_m (T_h - T_c) \tag{3.2}$$

Where Q_c is the heat flux from the cold side to the hot side and Q_h is the heat flux from the hot side of the Peltier Module. Using the performance graph supplied by the manufacturer the three unknown parameters a_m, R_m, and K_m were calculated. The model was simulated in COMSOL Multiphysics and compared with the manufacturer data to verify its function. In the simulation the Peltier module was placed between two aluminium plates acting as heat sinks. The plate at the hot side was kept at a constant temperature of 25°C. Figure 3.1 shows the simulation result of the Peltier model with the current through the Peltier set to 1.2 A.

Figure 3.2 shows the temperature gradient through the Peltier model with different currents.

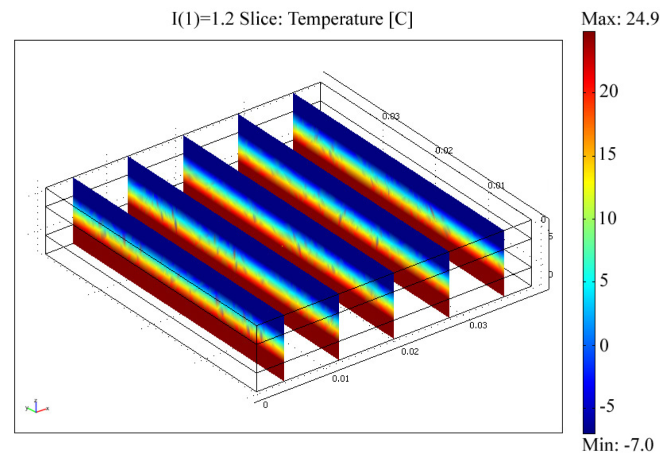

Figure 3.1: Simulation of the Peltier model in COMSOL Multiphysics.

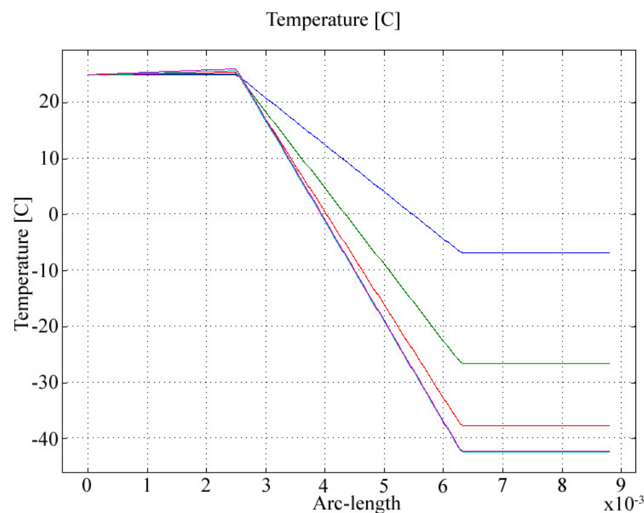

Figure 3.2: The temperature gradient through the Peltier model at currents from 1.7 to 8.5 A.

3.2 Model of the box and Peltier modules

The box model has the dimensions 250x250x100 mm and the outside of the box is covered by an insulated material. The insulation is represented by setting the thermal transfer of the box wall to a value calculated from the thickness of the insulation. The insulation used was ordinary Styrofoam used as insulation in houses with a thermal conductivity of 0,037 W/m°C. Inside the box a 10 mm thick aluminium heat spreader was attached to the bottom of the box. The purpose of the heat spreader is to stabilize critical electronics e.g. A/D converters and amplifiers which will be attached to the heat spreader. Less critical components e.g. a passive filters can be positioned in the air above the heat

spreader. On the outside of the box, against the bottom, the Peltier modules where attached. The exhaust side of the Peltier modules where then attached to a heat sink.

In the simulation the electronics were represented by four 50x50x1 mm silicon cubes placed on top of 50x50x2 mm alumina electrical insulation pad, positioned in each corner of the heat spreader. The total power dissipation was set to the estimated 10 W of the front-end and was distributed unsymmetrical over the four cubes inside the box as shown in figure 3.3(a).

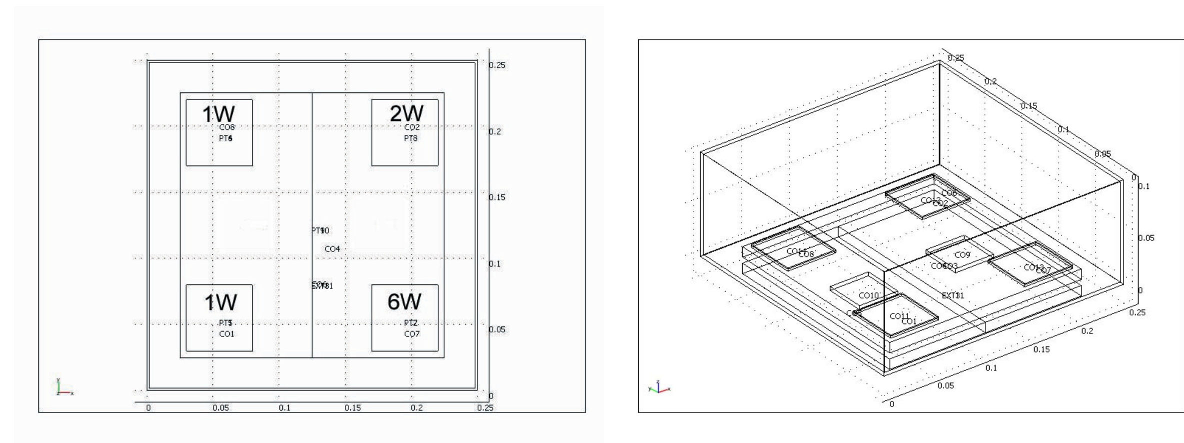

(a) *Distribution of the 10 W dissipated by the electronics.*

(b) *Simulation model of the box.*

Figure 3.3: Simulation setup.

3.2.1 Evaluation of the Peltier setup

In the first set of simulations different Peltier module setups where evaluated, in order to reduce the number of design alternatives for the following simulations. Three different Peltier setups were evaluated with, one, two and four Peltier modules. The Peltier modules were uniformly distributed over the bottom of the box in the different designs. The designs were evaluated by finding the lowest achieved temperature of the heat spreader at an ambient temperature of 40°C and by comparing the maximum temperature differences over the heat spreader. The heat sink on the exhaust side of the Peltier modules should not significantly exceed 70°C, this to avoid over heating the Peltier module. The simulation results for the different designs are displayed in table 3.1.

The lowest temperature, 1.5°C, is achieved with two Peltier modules, whereas the lowest temperature difference on the heat spreader 2.5°C is achieved when four Peltier modules are used. The design using two Peltier modules was considered to be the best

Table 3.1: Lowest achieved temperature of the different Peltier setups.

Nr of Peltier	Lowest temperature	Temperature difference of heat spreader	Exhaust temperature
1	20.6°C	4.3°C	69°C
2	1.5°C	3.0°C	71°C
4	5.6°C	2.5°C	75°C

compromise between the designs, this because the simulation model is believed to over estimate the heat transfer from the heat sinks. Further simulations are only conducted on the design using two Peltier modules.

3.2.2 Evaluation at different ambient temperatures

In the second and final simulation the selected design was exposed to different ambient temperatures while the centre of the heat spreader was kept at a constant 20°C by changing the current in the Peltier modules. The simulations were performed at three different ambient temperatures, 40°C, 0°C and -40°C.

With the ambient temperature set to 40°C the current through the two Peltier modules had to be set to 1.34 A to keep the centre of the heat spreader within 20°C. The maximum temperature difference of the heat spreader was measured to 2.7°C (see figure 3.4(b)) with a temperature gradient of the air inside the box from 20°C to 21.2°C. Figure 3.4 shows both the temperature gradient through the centre of the box and the temperature spread across the heat spreader.

When the ambient temperature was decreased to 0°C the Peltier modules changed from cooling to heating the box and a current of -0.35 A was needed to keep the centre of the heat spreader at 20°C. The maximum temperature difference of the heat spreader at this ambient temperature was measured to 2.0°C (see figure 3.5(b)). The air inside the box has a temperature gradient from 20°C to 19.6°C (see figure 3.5(a)).

With the ambient temperature further decreased to -40°C the current through the Peltier modules had to be -1.53 A for the centre of the heat spreader to be 20°C. The temperature difference of the heat spreader is further decreased to 1.8°C (see figure 3.6(b)). The air temperature gradient starts at 20°C and ends at 17.8°C (see figure 3.6(a)).

Some of the measurement data from the simulations are presented in table 3.2 to give a better overview. The maximum temperature difference at one point on the heat spreader over the temperature span 40°C to -40°C was 0.7°C this was measured over one of the Peltier modules. The maximum temperature difference of the component cube was measured to 0.5°C.

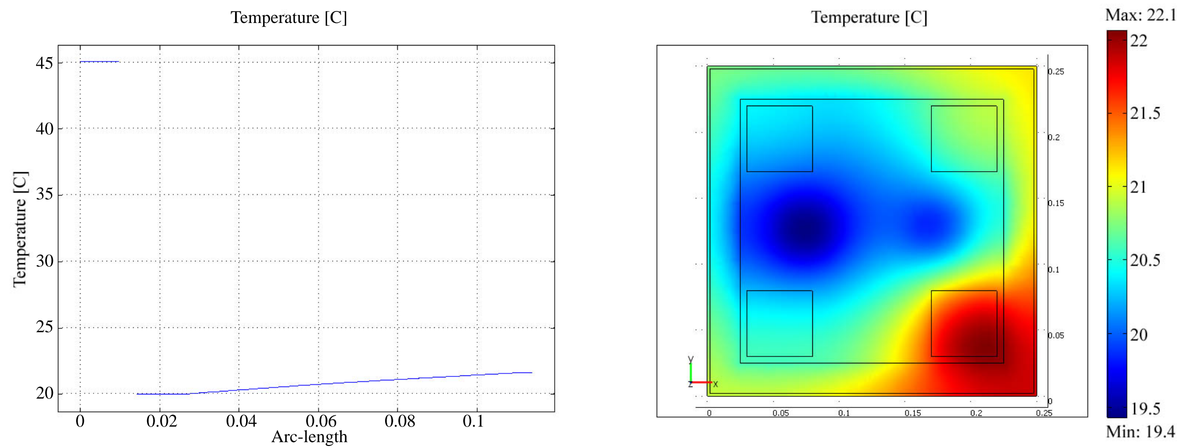

(a) *Temperature gradient through the centre of the box.* (b) *Temperature spread across the heat spreader.*

Figure 3.4: Simulation results at an ambient temperature of 40° C.

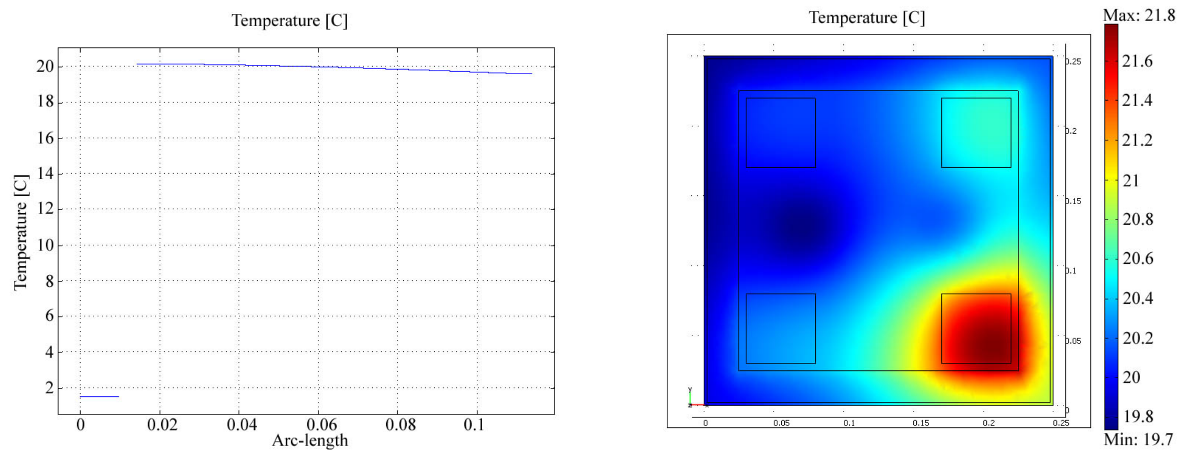

(a) *Temperature gradient through the centre of the box.* (b) *Temperature spread across the heat spreader.*

Figure 3.5: Simulation results at an ambient temperature of 0° C.

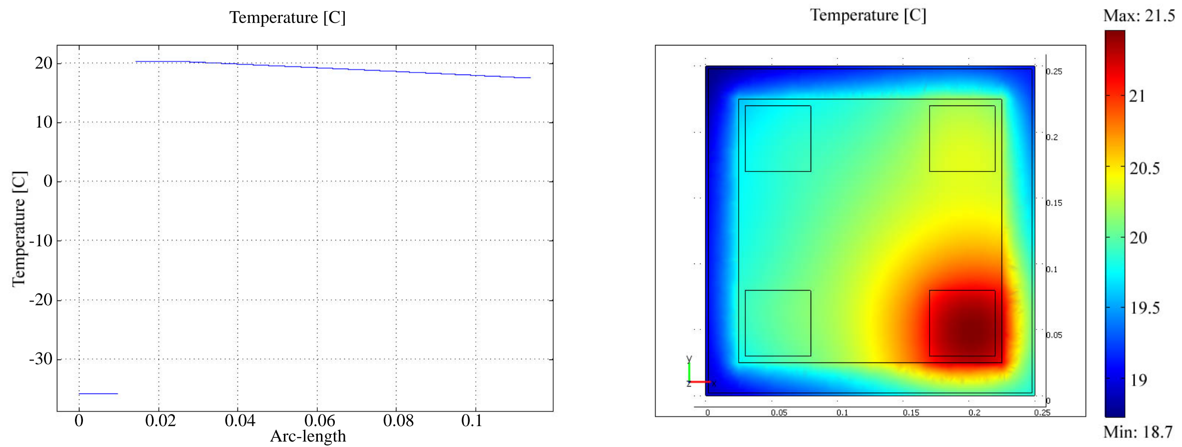

(a) *Temperature gradient through the centre of the box.* (b) *Temperature spread across the heat spreader.*

Figure 3.6: Simulation results at an ambient temperature of -40° C.

Table 3.2: An overview of the simulation measurement.

Ambient temperature	Current through Peltier modules	Temperature difference of heat spreader	Maximum exhaust temperature
40°C	1.34 A	2.7°C	45.5°C
0°C	-0.35 A	2.0°C	2°C
40°C	-1.53 A	1.8°C	-36°C

CHAPTER 4

Thermal Management Box

In this section the mechanical and electrical aspects of the manufactured prototype will be described.

4.1 The module

The prototype for the temperature-controlled module is based on the simulation model. The prototype consists of two fundamental parts; the aluminium box, in which the electronics will be positioned, and an outer casing made of insulation material. Figure 4.1 shows an illustration of the parts making up the complete module. First the insulation casing made of 70 mm thick Styrofoam which slots over the aluminium box. Inside the aluminium box the 10 mm thick aluminium heat spreader is attached to the bottom. The two Peltier modules are attached to the outside of the aluminium box. The Peltier modules used are two PE-127-14-15-S from the manufacturer Supercool, which have a maximum transfer capacity of 59,4 W at the maximum temperature difference of 74°C. Between the Peltier modules and the heat sinks there are aluminium blocks with the dimensions 40x40x20 mm, which make room for a 23 mm thick insulation layer between the box and the heat sinks. In each of the two aluminium blocks a temperature sensor is fitted to measure the temperature of the exhaust side of the Peltier modules. Two heat sinks are used, one for each Peltier module. The heat sinks have a base of 216x100 mm, fin width and fin height were 4 mm and 67 mm, respectively. Figure 4.2 shows a picture of the finished prototype box.

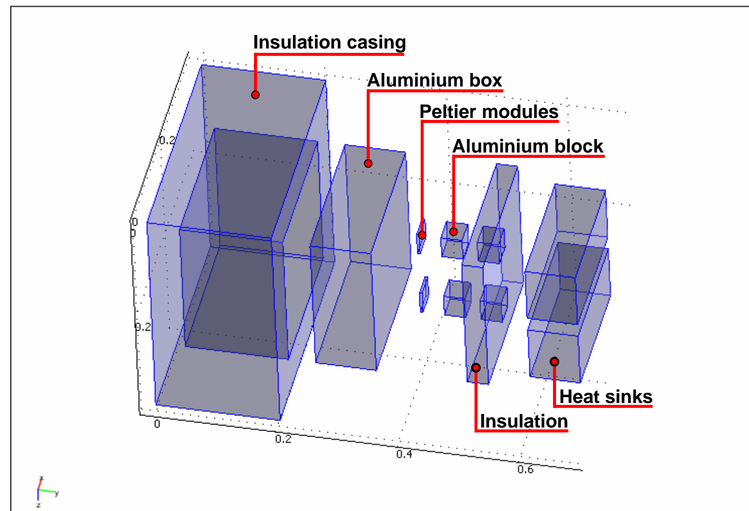

Figure 4.1: Part illustration of the prototype Box.

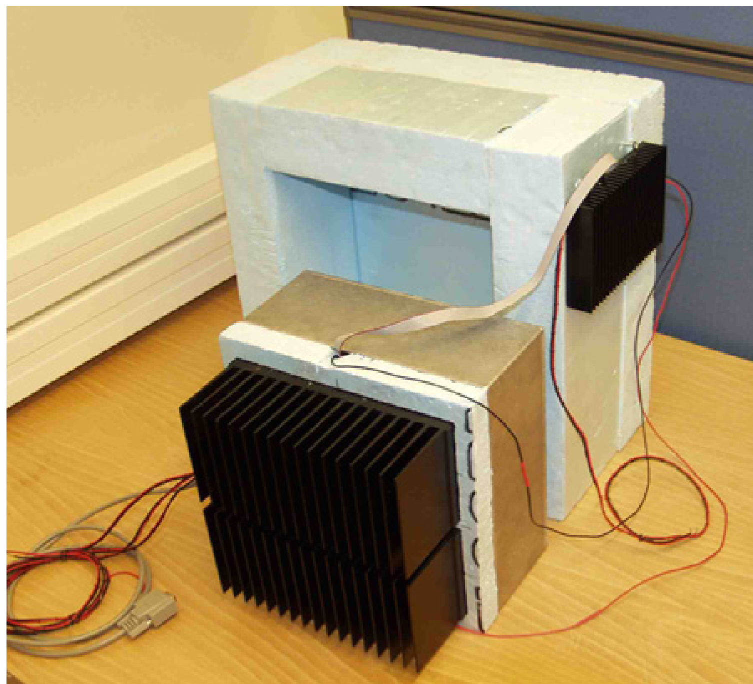

Figure 4.2: Picture of the finished prototype box.

4.2 Temperature controller

Figure 4.3 shows a simple block diagram of the temperature controller and driver for the Peltier module. The temperature controller is based on an ATmega128 8-bit microcontroller from Atmel.

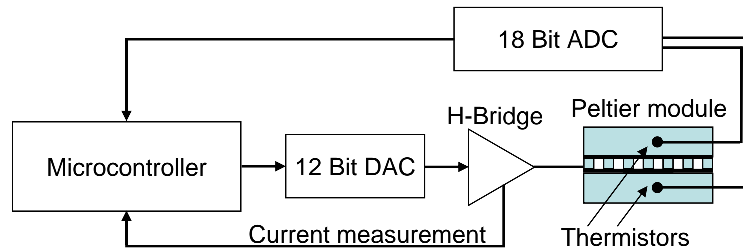

Figure 4.3: Block diagram of temperature controller

The temperature control system consists of three temperature sensors, one measures the temperature of the aluminium heat spreader inside the box and the other two measures the exhaust temperature of the two Peltier modules. The sensors are sampled by an ADC connected to the microcontroller. The Peltier modules are driven using a linearly controlled H-bridge interfaced to the microcontroller by a DAC. The separate parts of the control system are described in more detail in the following sections, beginning with the temperature sensor and then moving through the complete chain to the driving H-bridge.

4.2.1 Temperature sensor

The temperature sensor measuring the temperature of the heat spreader was an ACC-004 10 kΩ NTC thermistor from RTI Electronics. This type of thermistor is factory trimmed to match within ±0.2°C over the range 0-70°C. In air the thermistor has a thermal time constant of 10 s and a heat dissipation constant of 1 mW/°C. The thermistor is biased through a 10 kΩ ±0.1 % ±25 ppm/°C resistor, from a 2.5 V ±0.275 % precision voltage reference LT1790. This gives a dissipation of 156 μW in the thermistor which gives about 0.17°C of self heating in air. The two sensors used for the exhaust temperature were Mitsubishi type RH16 10 kΩ thermistors with a heat dissipation constant of 0.6 mW/°C in air. The two thermistors where biased in the same way through a 10 kΩ resistor which gives about 0.26°C of self heating in air.

The ADC used to read the voltage over the thermistors is the MAX1400 sigma-delta ADC from Maxim. The thermistors are connected to the ADC through a simple RC anti-alias filter. The sensors are calibrated against a F250 MkII Precision Thermometer with a full range accuracy of ±0.01°C. The temperature is sampled at a one degree interval over the range from -12°C to 76°C and then used to form a cubic spline interpolation table below -12°C a linear approximation is used. The resolution of the temperature sensors is 0.0008°C and an accuracy relative the precision thermometer of ±0.1°C is achieved over the range -12°C to 70°C.

4.2.2 The control loop

A PI-control algorithm was implemented on the microcontroller. The design around the microcontroller is entirely conventional, for more details see the ATmega128 manual [14]. The PI-controller has one real-time input, the temperature of the heat spreader. The exhaust temperature is used to detect overheating of the Peltier modules and for evaluation purposes, not as an input to the temperature controller. The 20°C set point is a fourth input. Using the set point and the heat spread temperature, a desired current for the H-bridge is calculated which is passed to the H-bridge-controller with an update frequency 1 Hz.

To prevent integrator windup, thus speed up the recovery from transients, the size of the integral term is reduced by using a feedback system. The feedback system compares the actual current through the Peltier module and the desired current scaling the difference and adding it to the integral term. Figure 4.4 shows a diagram of the PI-controller.

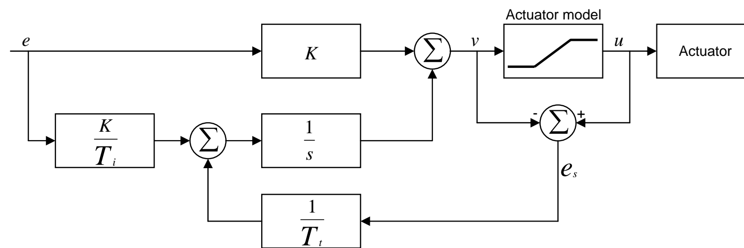

Figure 4.4: PI-controller with antiwindup.

4.2.3 The output drive

The H-bridge-controller is a separate PI-controller controlling the current through the Peltier modules. The H-bridge-controller has two inputs; the desired set point from the main PI-controller and the current through the Peltier modules obtained by measuring the voltage over a shunt resistor in the H-Bridge, using an INA122 instrumentation amplifier and the 10-bit ADC integrated in the microcontroller. From these two inputs a 12-bit value is calculated representing the output voltage of the 12-bit DAC connected to the microcontroller. The DAC is the 12-bit MAX252 from Maxim configured to have a rail-to-rail (0-5 V) output voltage [15]. The sample rate of the H-bridge-controller is 100 Hz. The circuit diagram for the H-bridge is shown in figure 4.5. The circuit consists of the H-bridge transistors and the current measuring device.

The two lower MOSFETs are linearly controlled by the DAC. For the two upper MOSFETs the control is strictly done in an on/off manner from two separate I/O pins on the microcontroller. The current through the Peltier module is obtained by measuring

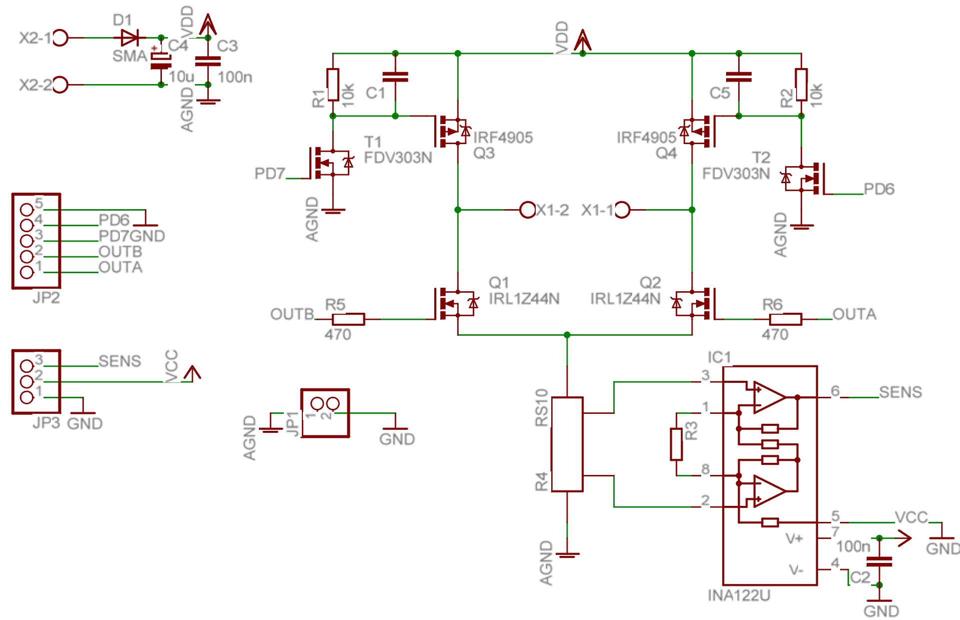

Figure 4.5: Circuit diagram for the H-bridge.

the voltage over a shunt resistor. The voltage across the resistor is amplified by the instrumentation amplifier with a gain of about 100, giving the scale 1 A/V and the range from 0-5 A.

One disadvantage when using a linear driver is the heat dissipation. This can be prevented using a PWM (Pulse Width Modulation) H-bridge, but high-current switching can generate substantial radio-frequency interference at the sensor and surrounding electronics. Because the electronics housed in the box is an antenna sensor front-end which has high demands in regards to noise, the linear approach was chosen despite its disadvantages.

The main control electronics consisting of the microcontroller, the ADC and the DAC are positioned on a circuit board inside the box. The H-bridge is attached to the outside of the insulation casing, this because the heat dissipated by it. If the H-bridge is positioned inside the box the Peltier modules has to work much harder. The decision to leave the H-bridge outside the box results in its exposure to the temperature change in the exterior environment. This will influence the properties of the H-bridge, but because of the current PI-control loop this will not significantly affect the current through the Peltier modules.

4.3 Matlab GUI

As a user interface to the controller a simple Matlab GUI (Graphical user interface) was made. The GUI makes it possible to change the temperature set point for the controller. It is also possible to change the parameters for the PI-controller both for the temperature control loop and the current control loop. When the controller is in active mode the measured temperature and current is displayed and plotted in a graph, the data is also saved in a file. The main function of the GUI is to use it when tuning and evaluating the controller. Figure 4.6 shows the GUI window.

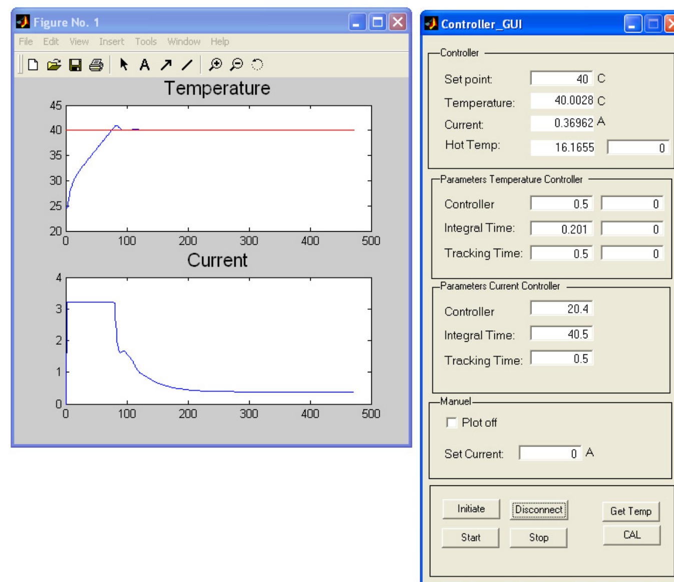

Figure 4.6: The Matlab GUI inteface to the controller.

Chapter 5

Final Evaluation of the Finished Prototype

To evaluate the performance of the prototype a climate chamber was used, in which the module was exposed to different temperatures. Figure 5.1 shows the evaluation setup consisting of the climate chamber with a stability of $\pm 2°C$, an F250 MkII Precision Thermometer for measuring the temperature inside the climate chamber (all other temperatures are measured by the temperature sensors used by the control system), a computer for logging data using a Matlab GUI, and power supplies. Inside the box two power resistors were used to generate the estimated power dissipation of 10 W. In this section the different measurements and results are described.

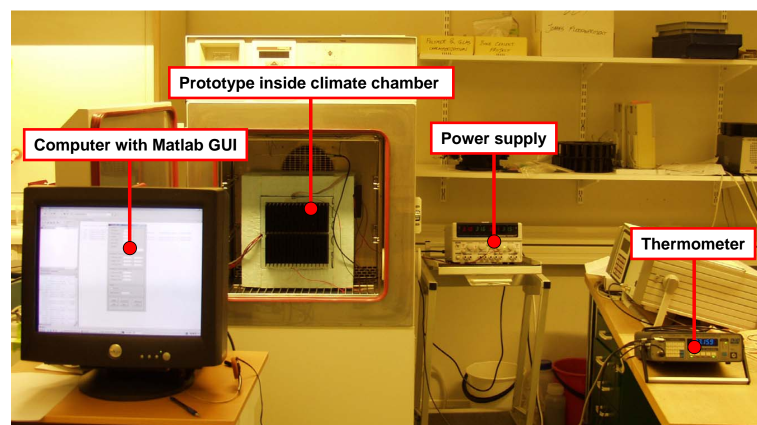

Figure 5.1: Evaluation setup.

5.1 Evaluation with ambient temperature changes

The ability to manage temperature changes in the ambient air was evaluated by exposing the box to temperature changes from 40°C down to -40°C over a time period of 5.5 hours. Figure 5.2(a) shows the temperature cycle of the program. The power dissipation inside the box is a constant 10 W. Figure 5.2(b) shows the measured temperatures of the aluminium heat spreader, the air inside the box and the ambient air.

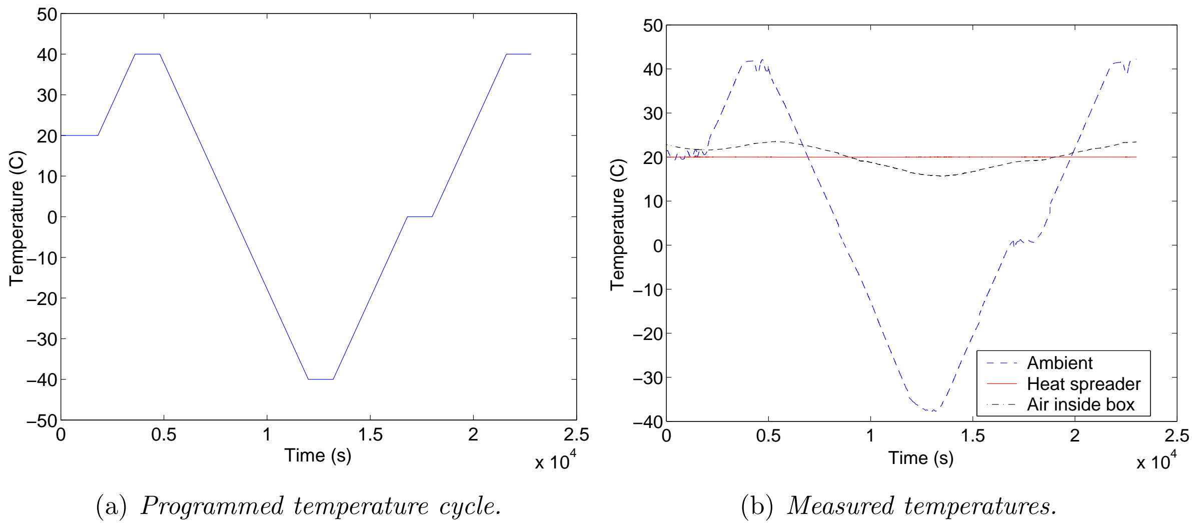

(a) *Programmed temperature cycle.* (b) *Measured temperatures.*

Figure 5.2: Temperature cycle and measured temperatures during ambient temperature changes.

Figure 5.3 shows a closer view of both the temperature of the aluminium heat spreader and the air inside the box. The centre point of the heat spreader is kept at 20°C with minor deviations of ±0.02°C. The air measured 45 mm above the aluminium heat spreader shows temperature variations of ±5°C.

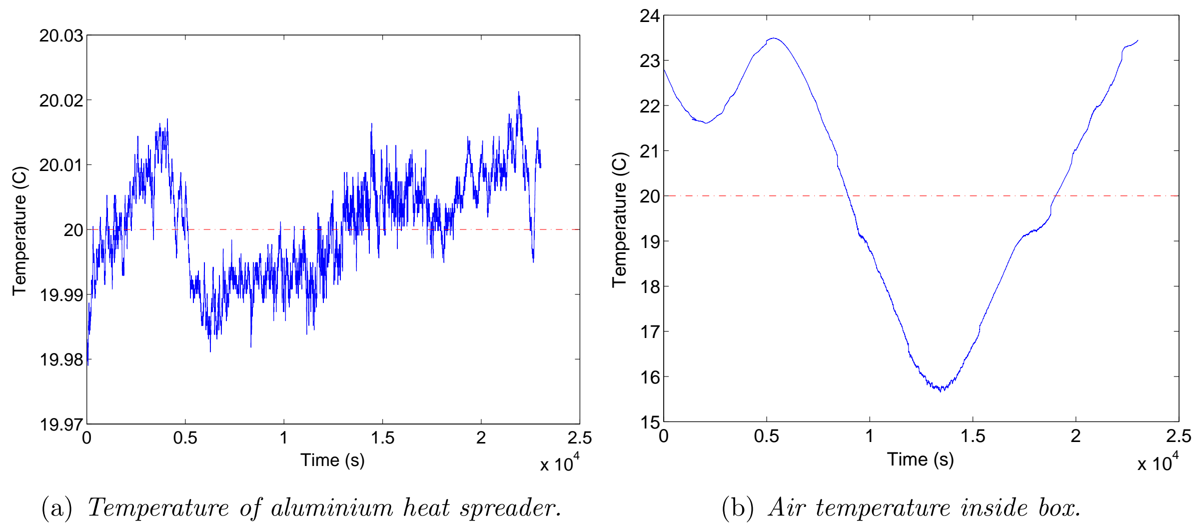

(a) *Temperature of aluminium heat spreader.* (b) *Air temperature inside box.*

Figure 5.3: Closer view of measured temperatures inside the box.

The exhaust side temperature measured in the aluminium block between the Peltier module and the heat sink is about 5°C higher than the ambient temperature. This is illustrated by the graph in figure 5.4.

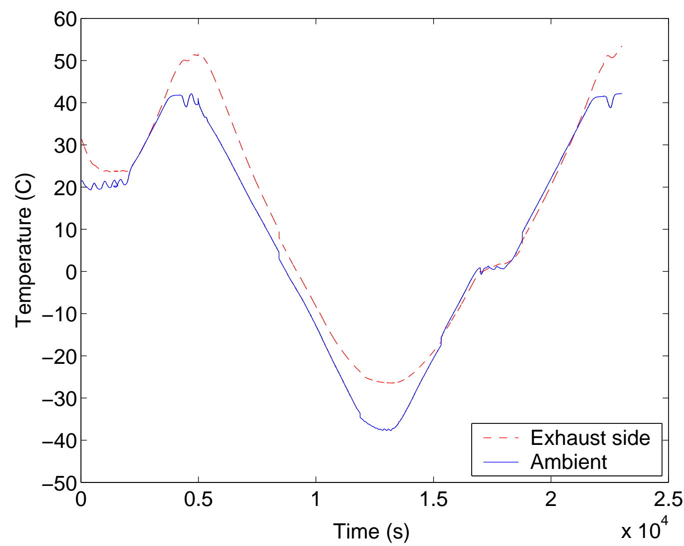

Figure 5.4: Exhaust temperature plotted against the ambient temperature.

5.2 Evaluation of recovery from power dissipation changes

The ability to recover from changes in internal power-dissipation was evaluated by switching the power dissipated inside the box on and off in different time intervals. The ambient temperature during this evaluation was 20°C. Figure 5.5(a) shows the measured temperature of the heat spreader, with a maximum temperature peak of ±0.06°C from the nominal 20°C, the duration of the peaks is about 400 s. The air inside the box showed maximum deviation of about ±1°C see figure 5.5(b).

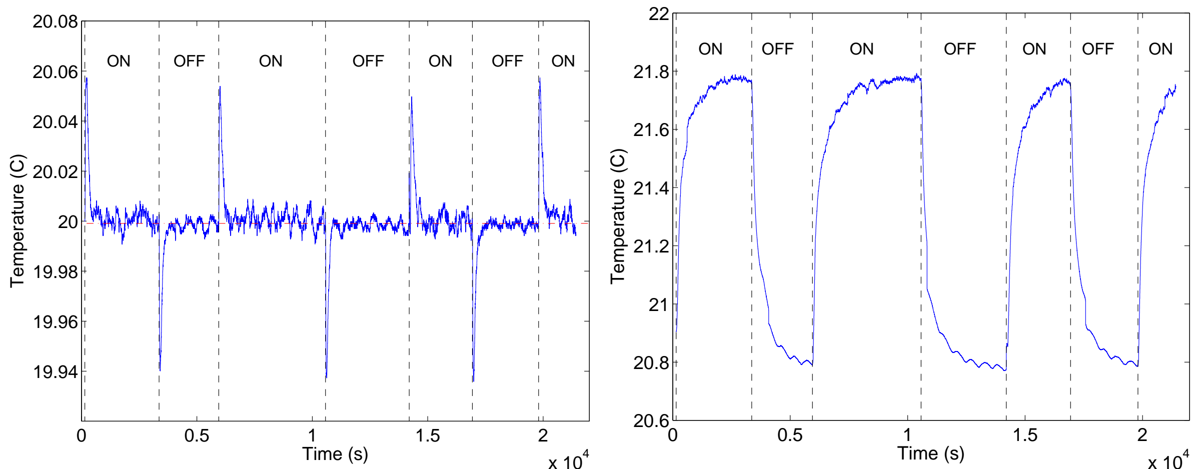

(a) *Measured heat spreader temperature under power dissipation changes.*

(b) *Measured air temperature under power dissipation changes.*

Figure 5.5: Measured temperature under power recovery test.

5.3 Evaluation of stability at constant power dissipation

The stability of the system was investigated by exposing the box to the two extreme temperatures -40°C and 40°C during a 3 hour time period. The power resistors inside the box gave a constant power dissipation of 10 W.

With the ambient temperature at -40°C, the measured temperature of the aluminium heat spreader stabilizes at 20°C with minor deviations of ±0.01°C see figure 5.6. The air temperature stabilizes at 16.6°C with deviations of ±0.08°C see figure 5.6(b).

When the ambient temperature was changed to 40°C the upper limitations of the box functionality was reached. As can be seen in figure 5.7(a) the system started out fine but

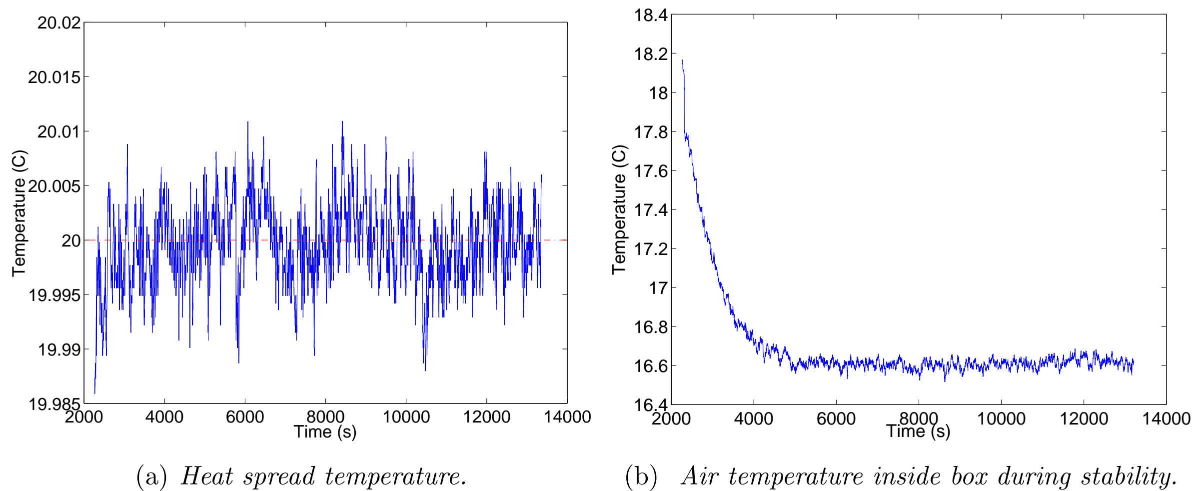

(a) *Heat spread temperature.* (b) *Air temperature inside box during stability.*

Figure 5.6: Measured temperature during stability evaluation at an ambient temperature of -40° C.

at about 12000 s in to the test a "thermal run away" happens. Both the aluminium heat spreader and the air show a steady increase in temperature. The "thermal run away" is caused by the temperature increase of the exhaust heat sinks (see figure 5.7(b)). The exhaust temperature gradually increases. When a temperature of 59°C is reached the performance Peltier modules decrease rapidly and the Peltier modules produce more heat than it can transfer, which causes the rapid heating of the system.

When the power dissipation inside the box was reduced to 8.5 W at an ambient temperature of 40°C, the "thermal run away" was no longer a problem. The exhaust temperature stabilizes at 52°C and the aluminium heat spreader temperature stabilizes at 20°C with deviations of ±0.01°C. The air temperature stabilizes at 23°C.

To verify that it is the temperature of the exhaust side of the Peltier modules that limits the system, the box was rotated in the climate chamber so that the fan inside the chamber produced an air flow through the heat sink. The ambient temperature was still 40°C, the power dissipation inside the box was set to the prior value of 10 W. The air flow from the fan kept the exhaust side temperature at about 49°C. The reduction of exhaust temperature improved the heat-transfer efficiency enough to allow operation at 10 W internal power dissipation. The aluminium heat spreader temperature stabilized at 20°C with deviations less then ±0.02°C see figure 5.8(a). The air temperature inside the box stabilized at 23.25°C (see figure 5.8(b)). The air flow from the fan kept the exhaust side temperature at about 49°C see figure 5.9.

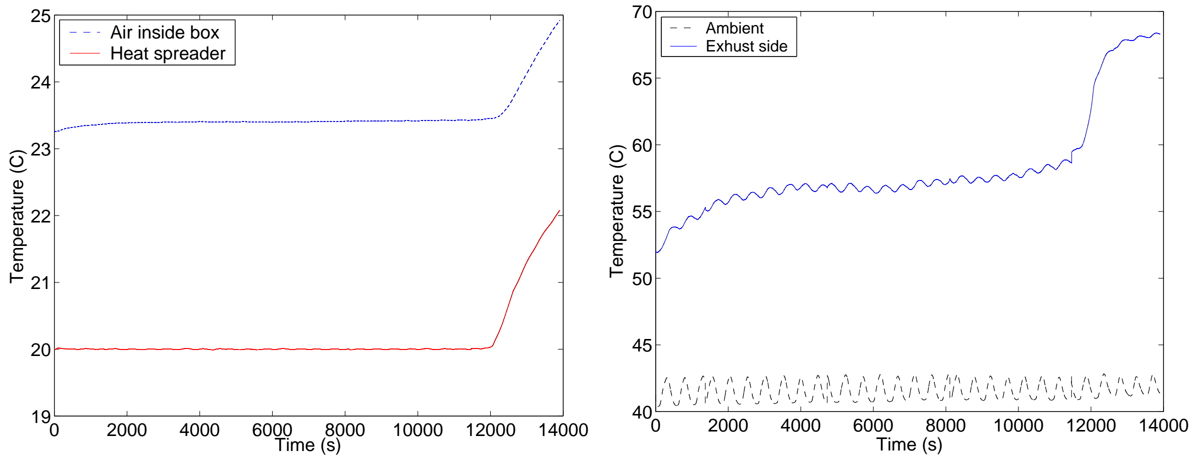

(a) *Temperature of heat spreader and air inside the box.* (b) *Measured Exhaust temperature.*

Figure 5.7: Measured temperature during stability evaluation at an ambient temperature of 40° C.

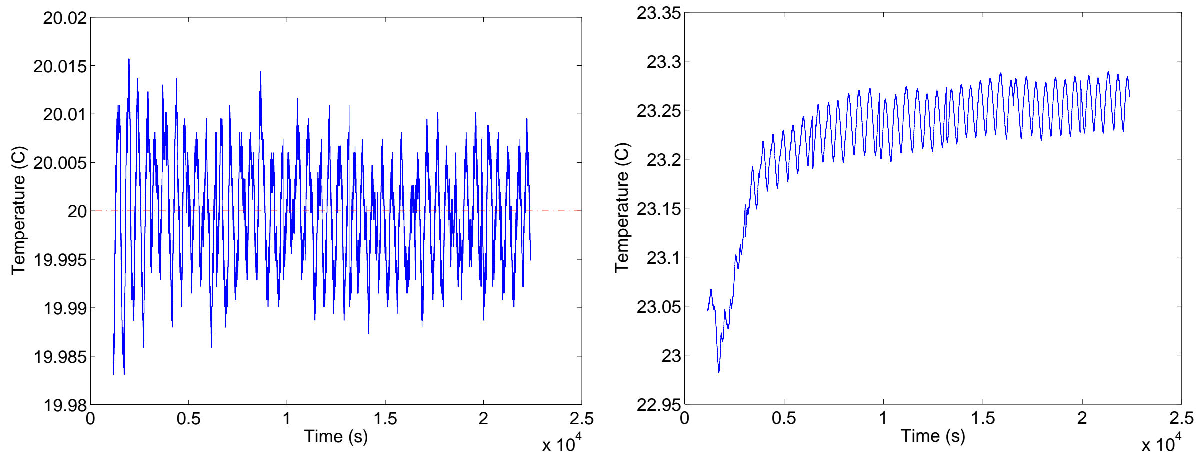

(a) *Heat spread temperature .* (b) *Air temperature inside box.*

Figure 5.8: Measured temperature at 10 W dissipation and ambient temperature 40° C with air flow.

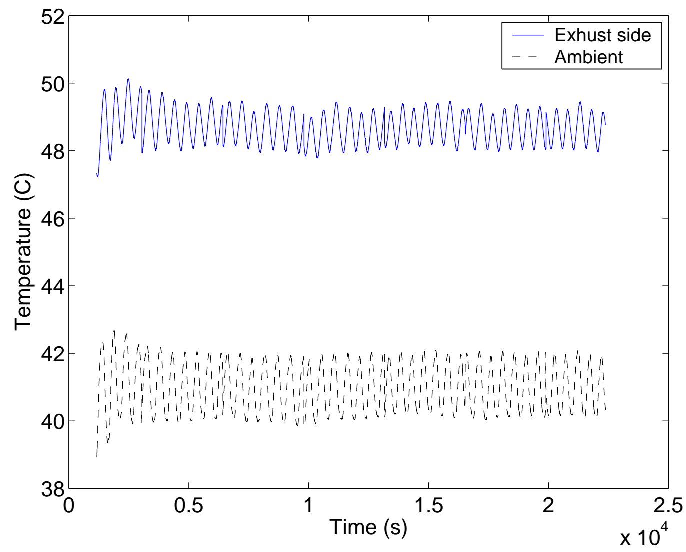

Figure 5.9: Exhaust side temperature at 10 W dissipation and ambient temperature 40° C with air flow.

CHAPTER 6

Discussion and Future Work

6.1 Discussion

The design of a temperature-stabilized module has been evaluated using simulations on which the final prototype was based. The prototype was evaluated under a series of different measurements. The performance under ambient temperature changes, stability and power change recovery was evaluated.

The simulations proved to be a useful initial study of the system where design matters such as Peltier module configuration were answered. When comparing the simulations with the measurements made on the real prototype box, the simulation model was found to some extent overestimate the performance of the system.

During the measurements on the prototype box it was discovered that the upper limits of the system was reached during the stability test at an ambient temperature of 40°C. The heat sink temperature exceeded 59°C and a "thermal run away" was recorded. This can be prevented by either reducing the power dissipation from the electronics or by increasing the heat transfer from the heat sink by adding larger heat sinks. As a safety measure the temperature controller will automatically turn off if the exhaust temperature reaches 57°C. The outdoor temperature of northern Scandinavia rarely reaches 40°C, if the heat sink is positioned in the shade with no direct sunlight this will not be a problem.

Both simulations and measurements show the feasibility of the proposed design, with temperature kept stable to ±0.02°C. Critical parts can be attached to the aluminium heat spreader while less critical can be positioned above the heat spreader. The actual temperature stability of the electronics attached to the heat spreader is highly dependent on the thermal resistance between the component and the heat spreader. Therefore packaging material and electrical-insulation material must be chosen with low thermal resistance.

The use of a completely enclosed box protects the electronics from the external environment e.g. dust and moisture. The system could be further improved by customizing the exhaust heat sink and the internal heat spreader.

6.2 Future work

Because the antenna front-end electronics was in the development stage during the construction and evaluation of the module, it was not possible to verify the function with the actual front-end electronics. The evaluation of whether the system can be used for temperature stabilization of the real antenna front-end has to be made.

When the electronics of the antenna front-end are known, more detailed simulations and tests can be made. This will show whether the system is suitable and in this stage it can also be useful to investigate if the use of spot cooling can improve the stability of critical parts of the front-end. With the knowledge of the shape and the thermal requirements of the antenna front-end it will be possible to make a more adapted design. It can also be useful to investigate different kinds of insulation with the aim of reducing the size of the box and still get a good insulation against the environment.

REFERENCES

[1] EISCAT Scientific Association. (2006, Mar.) EISCAT. [Online]. Available: http://www.eiscat.se

[2] U. G. Wannberg, *EISCAT 3D Design Specification Document, FP6-2003-Infrastructures-4: EISCAT 3D Proposal #011920*. EISCAT, 2005.

[3] A. E. Bergles, "Evolution of cooling technology for electrical, electronic, and microelectronic equipment," *IEEE Transactions on Components and Packaging Technologies*, vol. 26, no. 1, pp. 6–15, 2003.

[4] N. T. Larsen, "50 microdegree temperature controller," *Rev. Sci. Instrum.*, vol. 39, no. 1, 1968.

[5] J. M. A W Sloman, Paul Buggs and D. Stewart, "A microcontroller-based driver to stabilize the temperature of an oprical stage to within 1 mK in the range 4-38°C, using a Peltier heat pump and a thermistor sensor," *Meas. Sci. Technol.*, no. 7, pp. 1653–1664, 1996.

[6] F. B. Luciano Di Fiore, "High accuracy digital temperature control for a laser diode," *Rev. Sci. Instrum.*, vol. 66, no. 8, pp. 4051–4054, 1995.

[7] J. Holman, *Heat transfer*. London: McGraw-HILL, 1992.

[8] *Cambion Thermoelectric Handbook*. Massachussetts, USA: Cambion Thermionic Corporation, 1972.

[9] W. C. Carter. (2002) Mit 3.21 kinetic processes in materials. Internet draft. [Online]. Available: http://pruffle.mit.edu/c̃carter/3.21/Lecture_03_oneside.pdf

[10] D. Rowe, *CRC handbook of thermoelectrics*. Boca Raton: CRC Press, 1995.

[11] Tellurex Corporation. (2006, Mar.) An introduction to thermoelectrics. [Online]. Available: http://www.tellurex.com

[12] J. Fraden, *Handbook of Modern Sensors, Physics, Designs, and Applications*, 3rd ed. New York: Springer-Verlag, 2003.

[13] J. W. Ramon Pallas-Areny, *Sensors And Signal Conditioning*, 2nd ed. New York: John Wiley & Sons, 2001.

[14] *8-bit AVR Microcontroller with 128K In-System Programmable Flash, ATmega128*, 246N-AVR-03/06, Atmel, 2006.

[15] *Low-Power, Quad, 12-Bit Voltage-Output DAC with Serial Interface*, Maxim, 2002.